Computational Materials Science 259 (2025) 114114

Contents lists available at ScienceDirect

Computational Materials Science

journal homepage: www.elsevier.com/locate/commatsci

Full length article

Valence electron concentration-dependent stability of $L1_2$, $D0_{23}$, and $D0_{22}$ ordered phases in high-entropy alloys

Hiroshi Mizuseki [a], Ryoji Sahara [b], Kenta Hongo [c,*]

[a] Korea Institute of Science and Technology (KIST), Seoul 02792, Republic of Korea
[b] National Institute for Materials Science (NIMS), Tsukuba 305-0047, Japan
[c] Research Center for Advanced Computing Infrastructure, JAIST, Asahidai 1-1, Nomi, Ishikawa 923-1292, Japan

ARTICLE INFO

Keywords:
Semi-ordered atomic arrangements
Multicomponent alloys
Multi-principal element alloys
Order–disorder competition
First-principles calculations

ABSTRACT

We investigate the valence electron concentration (VEC) dependence of semi-ordered phases (SOPs) in high-entropy alloys (HEAs) via first-principles calculations. Fifteen equiatomic quaternary alloys composed of Al, Fe, Co, Ni, Cu, and Zn, along with non-equiatomic CrFeCoNi alloys, are analyzed. Formation energies of $L1_2$, $D0_{22}$, $D0_{23}$, and random solid solution (RSS) phases are evaluated. The results reveal that SOPs consistently exhibit lower formation energies than RSS. Although $D0_{23}$ phases have not yet been experimentally observed in HEAs, they are predicted to stabilize in specific intermediate VEC regions depending on composition, bridging the stability regimes of $L1_2$ and $D0_{22}$. These findings clarify VEC-dependent stability trends and provide insights into conditions favoring $D0_{23}$ formation in HEAs.

1. Introduction

Ordered phases such as $L1_2$ and $D0_{22}$ in intermetallic compounds are known to correlate closely with valence electron concentration (VEC). A clear VEC-dependent competition between $L1_2$ and $D0_{22}$ phase stability has been demonstrated in binary alloys like Pd_3X and Pt_3X (X = 3d transition metals) [1] and pseudobinary alloys like $(Pt,Rh)_3V$, $(Pd,Rh)_3V$, and $Pt_3(V,Ti)$ [2]. However, the stability of ordered phases in high-entropy alloys (HEAs) remains largely unexplored.

HEAs are traditionally considered random solid solutions (RSS) [3–7]. Nonetheless, experimental studies recently suggest local ordering, particularly involving $L1_2$ or $D0_{22}$ precipitates enhancing mechanical properties [8–12], though these studies mainly focus on multi-phase HEAs rather than single-phase ordered structures. As for the single-phase case, Niu et al. [13] first identified Cr-based $L1_2$ ordering in CrFeCoNi both experimentally and theoretically, while our previous work theoretically demonstrated stabilization of $L1_2$ and $D0_{22}$ phases in 3d transition-metal HEAs [14]. In binary alloys, it has been well known that the long-period $D0_{23}$ structure consisting of alternating stacking of $L1_2$ and $D0_{22}$ layers emerges [15]. However, the existence of long-period $D0_{23}$ phases in HEAs remains unexplored. Since direct experimental observation of atomic-scale ordering in such phases is challenging, this study aims to clarify their stability and the conditions under which they form through first-principles simulations.

This study systematically examines the stability of FCC semi-ordered phases (SOPs: $L1_2$, $D0_{22}$, and $D0_{23}$) in HEAs via first-principles calculations. We evaluate (i) 15 equiatomic quaternary alloys across a VEC range of 7.50 to 10.50 and (ii) $Cr(Fe,Co,Ni)_3$ non-equiatomic alloys (Cr backbone) across a more controlled VEC range of 7.78 to 8.72 for more detailed analysis, clarifying VEC-dependent trends and identifying conditions favorable for $D0_{23}$ stabilization. In high-entropy alloy (HEA) systems, VEC has been reported to correlate with the stable crystal structure [16,17]: a single FCC phase tends to form when VEC exceeds 8.00, a single BCC phase appears when VEC is below 6.87, and a mixture of FCC and BCC phases is observed in the intermediate range ($6.87 < VEC < 8.00$). Accordingly, in this study, all investigated compositions are assumed to adopt a single FCC structure, and the possible formation of BCC phases is neglected.

2. Computational methods

We performed spin-polarized density functional theory (DFT) calculations using VASP [18,19] with the PBEsol exchange–correlation functional [20] and projector-augmented wave pseudopotentials [21,22]. Crystal structures were modeled using $4 \times 4 \times 4$ FCC supercells containing 256 atoms. Ten random configurations were generated per composition to account for statistical variations [14,23]. Brillouin zone sampling used a $1 \times 1 \times 1$ Monkhorst–Pack k-grid and cut-off energies

* Corresponding author.
E-mail address: kenta_hongo@mac.com (K. Hongo).

https://doi.org/10.1016/j.commatsci.2025.114114
Received 9 June 2025; Received in revised form 5 July 2025; Accepted 9 July 2025

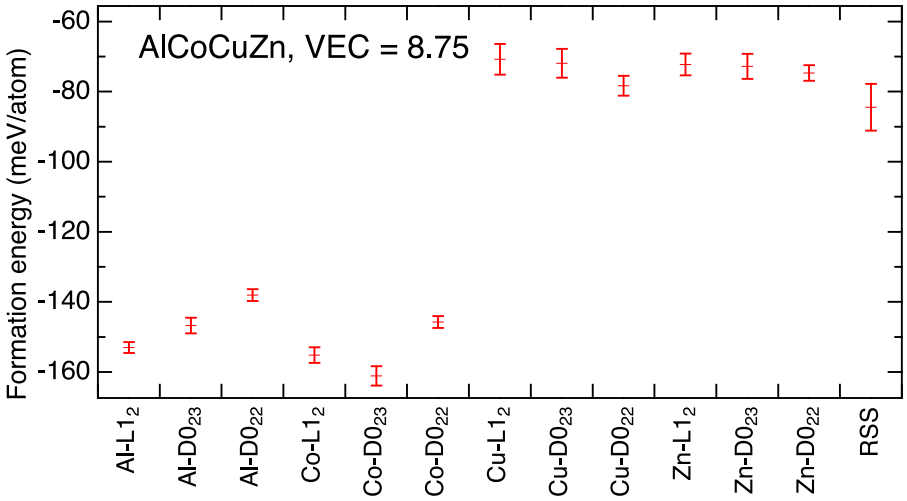

Fig. 1. Phase stability comparison of SOPs and RSS in AlCoCuZn. Formation energies of 12 semi-ordered structures (SOPs) and a random solid solution (RSS) for the equiatomic AlCoCuZn alloy. SOPs are constructed by assigning each of the four constituent elements to the ordered backbone sites in $L1_2$, $D0_{23}$, and $D0_{22}$ phases. Error bars represent standard deviations from 10 random configurations. In this case, SOP_1, SOP_2, and SOP_3 correspond to Co-$D0_{23}$, Co-$L1_2$, and Co-$D0_{22}$, respectively.

were set to the default values, validated by convergence tests. The convergence criteria for energy and force criteria were set to 10^{-4} eV and 10^{-3} eV/Å, respectively. Initial magnetic moments were assigned as follows: Al and Zn were treated as non-magnetic, Fe, Co, and Ni as ferromagnetic, and Cr as antiferromagnetic.

We modeled 15 equiatomic quaternary alloys composed of Al, Fe, Co, Ni, Cu, Zn, considering 12 possible SOPs ($L1_2$, $D0_{22}$, $D0_{23}$) and one RSS per alloy. The remaining 75% of the sites were occupied by the other three elements based on the simplified Warren-Cowley short-range order (WC-SRO) method [24] adopted in our previous study [14], thereby completing the structural models. For simplicity, SOPs are denoted using the label "X-SOP" (e.g., Co-$D0_{23}$, Al-$L1_2$ in Fig. 1), where the element X occupies the ordered sublattice positions, while the remaining elements are randomly distributed over the disordered sites. For instance, "Co-$D0_{23}$" represents a $D0_{23}$ structure in which Co atoms form the backbone of the ordered sublattice.

Additionally, we constructed CrFeCoNi non-equiatomic alloys by varying Fe, Co, Ni ratios while fixing the Cr content at 25 at.% to control the VEC. The ordered sites in SOPs were occupied by Cr atoms, and the remaining sites were randomly occupied by Fe, Co, and Ni atoms. Although the WC-SRO method was not applied here, we verified that the simple pseudo-random assignments yield formation energies (defined below) consistent with those obtained via WC-SRO within the statistical error, as confirmed for the equiatomic CrFeCoNi alloy.

In this study, the VEC is defined as the average number of valence electrons per atom for a given alloy, calculated as follows:

$$\mathrm{VEC} = \sum_i x_i v_i, \tag{1}$$

where x_i is the atomic fraction and v_i the number of valence electrons of element i. The conventional valence counts used were: Al (3), Cr (6), Fe (8), Co (9), Ni (10), Cu (11), and Zn (12). Using the DFT-based total energy for each structure, the formation energy per atom were obtained via:

$$E_f = E(\mathrm{HEA}) - \sum_i x_i E(X_i), \tag{2}$$

where E(HEA) is the total energy per atom of the alloy, and $E(X_i)$ the energy per atom of element i in its ground-state crystal structure (FCC Al, BCC Cr, BCC Fe, HCP Co, FCC Ni, FCC Cu, HCP Zn) [25,26].

3. Results and discussion

Fig. 1 shows the formation energies of AlCoCuZn as a representative case. Across all 15 equiatomic alloys, SOPs exhibit lower formation energies than RSS (details for others are Figures S2 in Supporting Information). Specifically, Co-$D0_{23}$ emerges as the most stable (SOP_1), followed by Co-$L1_2$ (SOP_2) and Co-$D0_{22}$ (SOP_3).

Hereafter, for convenience, the three SOPs corresponding to each HEA composition are labeled SOP_1, SOP_2, and SOP_3, in ascending order of formation energy. For instance, in Fig. 1, SOP_1, SOP_2, and SOP_3 in AlCoCuZn correspond to Co-$D0_{23}$, Co-$L1_2$, and Co-$D0_{22}$, respectively.

To further investigate the VEC-dependence, we introduce relative formation energy differences defined as:

$$\Delta E_f = E_f(\mathrm{SOP}_i) - E_f(\mathrm{SOP}_2); (i = 1 \text{ or } 3), \tag{3}$$

where SOP_2 is the reference, making ΔE_f negative for SOP_1, zero for SOP_2, and positive for SOP_3, enabling intuitive comparison.

Fig. 2 displays the relative formation energies ΔE_f for SOP_1 and SOP_3. $L1_2$ stabilizes at $7.75 \leq \mathrm{VEC} \leq 8.50$ and $\mathrm{VEC} \geq 9.50$, while $D0_{23}$ emerges at intermediate VECs (8.75, 9.00). $D0_{23}$ is predicted to stabilize between the $L1_2$ and $D0_{22}$ phases in a narrow VEC window, providing a new insight into semi-ordering in HEAs. This finding suggests VEC-guided pathways for engineering short-range order in FCC HEAs without changing the elemental types. Thus, as VEC increases, SOP_1 transits as $D0_{22} \rightarrow L1_2 \rightarrow D0_{23} \rightarrow L1_2$. This observation prompted a more detailed analysis of the conditions under which the $D0_{23}$ phase emerges.

To this end, CrFeCoNi non-equiatomic alloys were examined by varying Fe, Co, Ni compositions, keeping Cr at 25 at.%. This model can be regarded as a ternary alloy on the remaining 75 at.% sites. Note that previous studies confirmed equiatomic CrFeCoNi (VEC = 8.25) stabilizes Cr-$L1_2$ [13,14].

Fig. 3(a) shows that Cr-$L1_2$ and Cr-$D0_{22}$ coexist for $8.28 \leq \mathrm{VEC} \leq 8.31$, with Cr-$L1_2$ dominant at lower VEC (< 8.25) and Cr-$D0_{22}$ at higher VEC (> 8.47); Cr-$D0_{23}$ emerges around VEC = 8.28–8.41. The fine VEC resolution reveals transitions from Cr-$L1_2$ to Cr-$D0_{23}$ and then Cr-$D0_{22}$; large error bars near VEC = 8.35 reflect transition regions. Fig. 3(b) maps compositional regions favoring each SOP_1 phase: Cr-$L1_2$ and Cr-$D0_{22}$ dominate Fe-rich (low VEC) and Ni-rich (high VEC) regions, respectively, whereas Cr-$D0_{23}$ appears in intervening Co-rich (middle VEC) regions.

To verify generality, our results are compared with binary intermetallic compounds and pseudo-binary alloys (Table S2 in SI) [1,2,15,27]. Experimental data show $L1_2$ stabilizes at VEC = 8.25 and $9.25 < \mathrm{VEC} < 11.00$, and $D0_{22}$ at VEC = 8.50–8.75 [15]. Theoretical studies, including pioneering band-filling work by A. Bieber et al. [27], also demonstrate similar VEC dependencies. Our non-equiatomic results align with these trends.

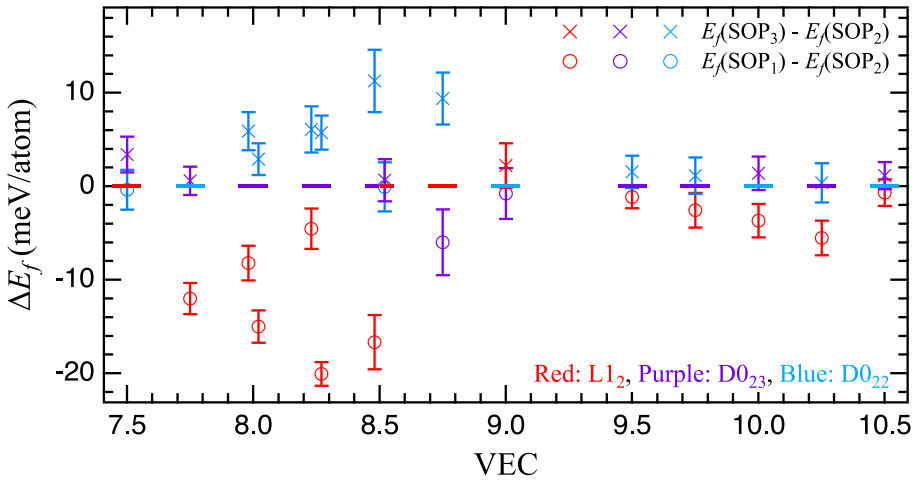

Fig. 2. VEC-dependent stability trend of SOPs across 15 equiatomic HEAs. Relative formation energies of SOP_1 (circles) and SOP_3 (crosses) with respect to SOP_2 for 15 equiatomic quaternary HEAs. Marker colors denote SOP types: red for $L1_2$, purple for $D0_{23}$, and blue for $D0_{22}$. SOP_1 transitions from $D0_{22}$ to $L1_2$ to $D0_{23}$ and then to $L1_2$ again with increasing VEC.

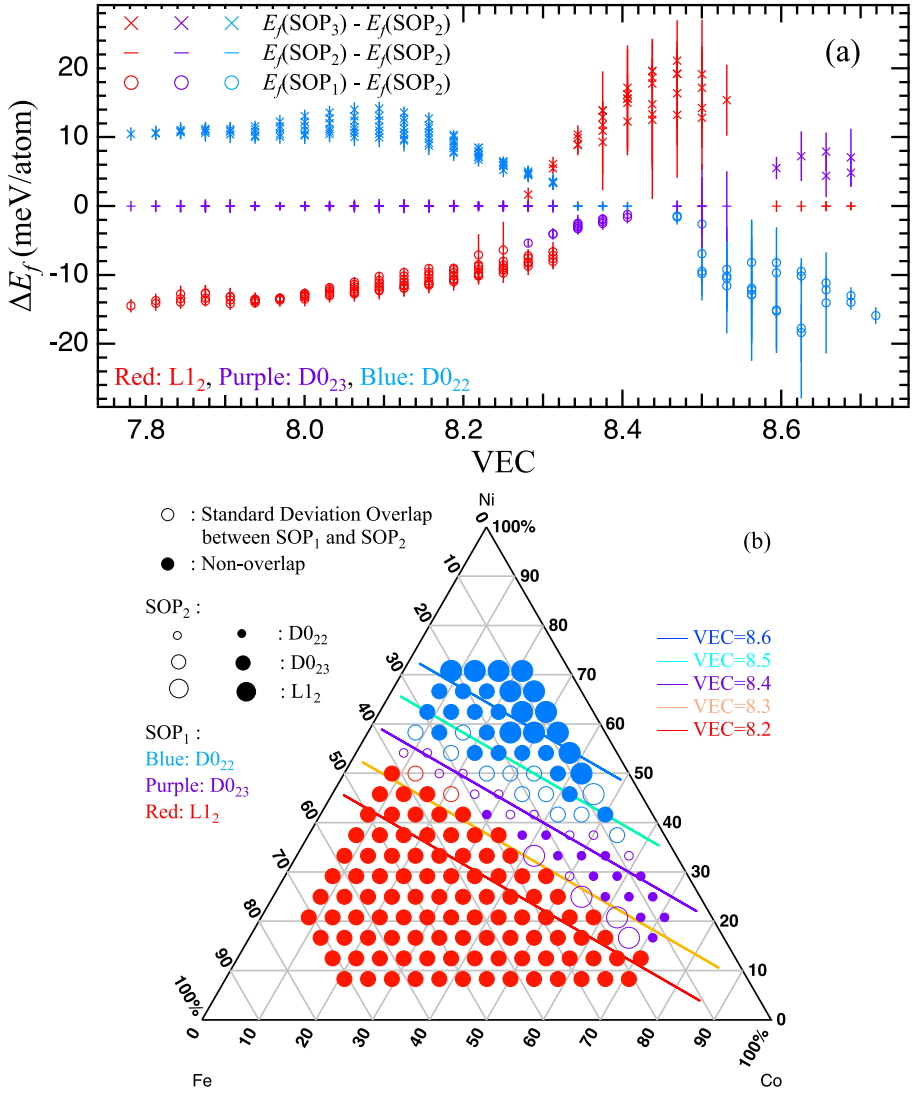

Fig. 3. Compositional and VEC effects on SOP stability in CrFeCoNi non-equiatomic HEAs. (a) Relative formation energies of SOP_1 and SOP_3 with respect to SOP_2 for CrFeCoNi alloys with varying Fe-Co-Ni ratios (Cr fixed at 25 at.%). Error bars denote standard deviations. (b) Compositional map showing SOP_1 stability regions projected onto the Fe-Co-Ni ternary plane. Marker colors represent phase type (red: Cr-$L1_2$, purple: Cr-$D0_{23}$, blue: Cr-$D0_{22}$), and marker size corresponds to SOP_2. Solid circles indicate statistically significant energy differences beyond the standard deviation, while open circles indicate overlaps.

In contrast, $D0_{23}$ is experimentally reported only at low VEC (VEC = 3.25) [15], with no reports in the studied range. This may raise doubts about its predicted stability; however, similar discrepancies between theory and experiment are well-known in binary systems. [28, 29]. First-principles calculations consistently show small energy differences (< 10 meV/atom) among the three phases. For instance, first-principles calculations for Al_3Ti predict $D0_{23}$ as the most stable, whereas experiments often observe $D0_{22}$ [15]. This is attributed to the fact that experimental results are influenced by kinetic factors and processing histories, often leading to the appearance of metastable $D0_{22}$ phases. Our predictions call for future experimental efforts, such as low-temperature annealing and advanced diffraction or microscopy techniques, to detect $D0_{23}$-like ordering in HEAs. Although our calculations predict $D0_{23}$ stability, experimental confirmation requires carefully controlled processing to selectively stabilize this phase.

4. Conclusion

In summary, our first-principles calculations for equiatomic quaternary alloys composed of Al, Fe, Co, Ni, and Cu, as well as for non-equiatomic CrFeCoNi alloys, revealed that the semi-ordered phases ($L1_2$, $D0_{23}$, $D0_{22}$) consistently exhibit lower formation energies than the random solid solution (RSS) in high-entropy alloys (HEAs). VEC-dependent stability trends indicate that $D0_{23}$ phases bridge the stability ranges of $L1_2$ and $D0_{22}$. The stabilization of $D0_{23}$ between $L1_2$ and $D0_{22}$ phases is supposedly attributed to its crystal structure incorporating features of both $L1_2$ and $D0_{22}$ (See Figure S1 and Table S1 for your eye guide). These results align with experimental trends observed in binary systems, reinforcing the role of VEC in governing ordered phase stability. Our findings extend these trends to HEAs and predict $D0_{23}$ stabilization in previously unexplored VEC regions. This finding suggests VEC-guided pathways for engineering short-range order in FCC HEAs without changing the elemental types. This study highlights VEC as a key factor governing the stability of ordered phases in HEAs and provides guidance for future experimental exploration of long-period ordered structures. Given that experimentally resolving atomic-scale arrangements in alloys requires significant effort, the insights obtained from this study are of considerable importance.

CRediT authorship contribution statement

Hiroshi Mizuseki: Writing – review & editing, Writing – original draft, Visualization, Validation, Methodology, Investigation, Funding acquisition, Formal analysis, Data curation, Conceptualization. **Ryoji Sahara:** Writing – review & editing, Validation, Resources, Methodology, Investigation, Funding acquisition, Formal analysis. **Kenta Hongo:** Writing – review & editing, Writing – original draft, Supervision, Software, Resources, Project administration, Methodology, Investigation, Funding acquisition, Formal analysis, Conceptualization.

Declaration of Generative AI and AI-assisted technologies in the writing process

During the preparation of this manuscript, the authors used ChatGPT o4 in order to improve its language and readability. After using this tool, all the authors reviewed and edited the content as needed and takes full responsibility for the content of the publication.

Declaration of competing interest

The authors declare that they have no known competing financial interests or personal relationships that could have appeared to influence the work reported in this paper.

Acknowledgments

This study was supported by the computational resources of the HPCI system [Project ID: hp230037, hp230468, hp240027], the JHPCN system [Project IDs: jh230038 and jh240026], Institute for Materials Research, Tohoku University [Proposal No. 202312-SCKXX-0502] and Numerical Materials Simulator at National Institute for Materials Science. The computations in this work have been partially performed using the facilities of the Research Center for Advanced Computing Infrastructure (RCACI) at JAIST. H.M. thanks the Korea Institute of Science and Technology, South Korea [Grant No. 2N62110, No. 2N64240, No. 2E33211, No. 2E33861] and Bilateral Collaboration Program through the National Research Foundation of Korea (NRF), South Korea [Grant No. 2021K2A9A2A0700009311]. R.S. acknowledges the financial support from JSPS KAKENHI [Grant No. 24K01149]. K.H. is grateful for financial support from MEXT-KAKENHI, Japan (JP19H05169 and JP23H04623), and the Air Force Office of Scientific Research, United States (Award Numbers: FA2386-20-1-4036 and FA2386-22-1-4065).

Appendix A. Supplementary data

Supplementary material related to this article can be found online at https://doi.org/10.1016/j.commatsci.2025.114114.

Data availability

Data will be made available on request.

References

[1] Z.W. Lu, B.M. Klein, A. Zunger, Spin-polarization-induced structural selectivity in Pd_3X and Pt_3X (X = 3d) compounds, Phys. Rev. Lett. 75 (1995) 1320–1323, http://dx.doi.org/10.1103/PhysRevLett.75.1320, URL https://link.aps.org/doi/10.1103/PhysRevLett.75.1320.

[2] E. Cabet, A. Pasturel, F. Ducastelle, A. Loiseau, $L1_2$-$D0_{22}$ competition in the pseudobinary (Pt, Rh)$_3$V, Pt$_3$(V, Ti), and (Pd, Rh)$_3$V alloys: Phase stability and electronic structure, Phys. Rev. Lett. 76 (1996) 3140–3143, http://dx.doi.org/10.1103/PhysRevLett.76.3140, URL https://link.aps.org/doi/10.1103/PhysRevLett.76.3140.

[3] J.-W. Yeh, S.-K. Chen, S.-J. Lin, J.-Y. Gan, T.-S. Chin, T.-T. Shun, C.-H. Tsau, S.-Y. Chang, Nanostructured high-entropy alloys with multiple principal elements: Novel alloy design concepts and outcomes, Adv. Eng. Mater. 6 (5) (2004) 299–303, http://dx.doi.org/10.1002/adem.200300567, arXiv:https://advanced.onlinelibrary.wiley.com/doi/pdf/10.1002/adem.200300567.

[4] E.P. George, W.A. Curtin, C.C. Tasan, High entropy alloys: A focused review of mechanical properties and deformation mechanisms, Acta Mater. 188 (2020) 435–474, http://dx.doi.org/10.1016/j.actamat.2019.12.015, URL https://www.sciencedirect.com/science/article/pii/S1359645419308444.

[5] M.-H. Tsai, J.-W. Yeh, High-entropy alloys: A critical review, Mater. Res. Lett. 2 (3) (2014) 107–123, http://dx.doi.org/10.1080/21663831.2014.912690.

[6] H. Shahmir, M.S. Mehranpour, S.A. Arsalan Shams, T.G. Langdon, Twenty years of the CoCrFeNiMn high-entropy alloy: achieving exceptional mechanical properties through microstructure engineering, J. Mater. Res. Technol. 23 (2023) 3362–3423, http://dx.doi.org/10.1016/j.jmrt.2023.01.181, URL https://www.sciencedirect.com/science/article/pii/S2238785423001746.

[7] W. Al Zoubi, R.A.K. Putri, M.R. Abukhadra, Y.G. Ko, Recent experimental and theoretical advances in the design and science of high-entropy alloy nanoparticles, Nano Energy 110 (2023) 108362, http://dx.doi.org/10.1016/j.nanoen.2023.108362, URL https://www.sciencedirect.com/science/article/pii/S2211285523001994.

[8] L. Liu, Y. Zhang, J. Li, M. Fan, X. Wang, G. Wu, Z. Yang, J. Luan, Z. Jiao, C.T. Liu, P.K. Liaw, Z. Zhang, Enhanced strength-ductility synergy via novel bifunctional nano-precipitates in a high-entropy alloy, Int. J. Plast. 153 (2022) 103235, http://dx.doi.org/10.1016/j.ijplas.2022.103235, URL https://www.sciencedirect.com/science/article/pii/S0749641922000225.

[9] Y.L. Zhao, T. Yang, Y.R. Li, L. Fan, B. Han, Z.B. Jiao, D. Chen, C.T. Liu, J. Kai, Superior high-temperature properties and deformation-induced planar faults in a novel $L1_2$-strengthened high-entropy alloy, Acta Mater. 188 (2020) 517–527, http://dx.doi.org/10.1016/j.actamat.2020.02.028, URL https://www.sciencedirect.com/science/article/pii/S1359645420301324.

[10] F. He, D. Chen, B. Han, Q. Wu, Z. Wang, S. Wei, D. Wei, J. Wang, C.T. Liu, J.-J. Kai, Design of $D0_{22}$ superlattice with superior strengthening effect in high entropy alloys, Acta Mater. 167 (2019) 275–286, http://dx.doi.org/10.1016/j.actamat.2019.01.048, URL https://www.sciencedirect.com/science/article/pii/S1359645419300631.

[11] J. Gan, J. Hou, T. Chou, X. Luo, J. Ju, J. Luan, G. Huang, B. Xiao, J. Zhang, J. Zhang, Y. Tao, J. Gao, T. Yang, A novel $D0_{22}$-strengthened medium entropy alloy with outstanding strength-ductility synergies over ambient and intermediate temperatures, J. Mater. Sci. Technol. 202 (2024) 152–164, http://dx.doi.org/10.1016/j.jmst.2024.02.057, URL https://www.sciencedirect.com/science/article/pii/S1005030224003487.

[12] T. Li, J.-X. Chen, T.-W. Liu, Y. Chen, J.-H. Luan, Z.-B. Jiao, C.-T. Liu, L.-H. Dai, $D0_{22}$ precipitates strengthened W-Ta-Fe-Ni refractory high-entropy alloy, J. Mater. Sci. Technol. 177 (2024) 85–95, http://dx.doi.org/10.1016/j.jmst.2023.07.069, URL https://www.sciencedirect.com/science/article/pii/S1005030223007806.

[13] C. Niu, A.J. Zaddach, A.A. Oni, X. Sang, J.W. Hurt, J.M. LeBeau, C.C. Koch, D.L. Irving, Spin-driven ordering of Cr in the equiatomic high entropy alloy NiFeCrCo, Appl. Phys. Lett. 106 (16) (2015) 161906, http://dx.doi.org/10.1063/1.4918996.

[14] H. Mizuseki, R. Sahara, K. Hongo, Order–disorder competition in equiatomic 3d–transition–metal quaternary alloys: phase stability and electronic structure, Sci. Technol. Adv. Mater.: Methods 3 (1) (2023) 2153632, http://dx.doi.org/10.1080/27660400.2022.2153632.

[15] T.B. Massalski, H. Okamoto, P.R. Subramanian, L. Kacprzak, Binary Alloy Phase Diagrams, second ed., ASM International, 1990.

[16] S. Guo, C. Ng, J. Lu, C.T. Liu, Effect of valence electron concentration on stability of fcc or bcc phase in high entropy alloys, J. Appl. Phys. 109 (10) (2011) 103505, http://dx.doi.org/10.1063/1.3587228.

[17] S. Guo, C.T. Liu, Phase stability in high entropy alloys: Formation of solid-solution phase or amorphous phase, Prog. Nat. Sci.: Mater. Int. 21 (6) (2011) 433–446, http://dx.doi.org/10.1016/S1002-0071(12)60080-X, URL https://www.sciencedirect.com/science/article/pii/S100200711260080X.

[18] G. Kresse, J. Furthmüller, Efficiency of ab-initio total energy calculations for metals and semiconductors using a plane-wave basis set, Comput. Mater. Sci. 6 (1) (1996) 15–50, http://dx.doi.org/10.1016/0927-0256(96)00008-0, URL https://www.sciencedirect.com/science/article/pii/0927025696000080.

[19] G. Kresse, J. Furthmüller, Efficient iterative schemes for ab initio total-energy calculations using a plane-wave basis set, Phys. Rev. B 54 (1996) 11169–11186, http://dx.doi.org/10.1103/PhysRevB.54.11169, URL https://link.aps.org/doi/10.1103/PhysRevB.54.11169.

[20] J.P. Perdew, A. Ruzsinszky, G.I. Csonka, O.A. Vydrov, G.E. Scuseria, L.A. Constantin, X. Zhou, K. Burke, Restoring the density-gradient expansion for exchange in solids and surfaces, Phys. Rev. Lett. 100 (2008) 136406, http://dx.doi.org/10.1103/PhysRevLett.100.136406, URL https://link.aps.org/doi/10.1103/PhysRevLett.100.136406.

[21] P.E. Blöchl, Projector augmented-wave method, Phys. Rev. B 50 (1994) 17953–17979, http://dx.doi.org/10.1103/PhysRevB.50.17953, URL https://link.aps.org/doi/10.1103/PhysRevB.50.17953.

[22] G. Kresse, D. Joubert, From ultrasoft pseudopotentials to the projector augmented-wave method, Phys. Rev. B 59 (1999) 1758–1775, http://dx.doi.org/10.1103/PhysRevB.59.1758, URL https://link.aps.org/doi/10.1103/PhysRevB.59.1758.

[23] C. Niu, C.R. LaRosa, J. Miao, M.J. Mills, M. Ghazisaeidi, Magnetically-driven phase transformation strengthening in high entropy alloys, Nat. Commun. 9 (1) (2018) 1363, http://dx.doi.org/10.1038/s41467-018-03846-0.

[24] Y. Ikeda, B. Grabowski, F. Körmann, Ab initio phase stabilities and mechanical properties of multicomponent alloys: A comprehensive review for high entropy alloys and compositionally complex alloys, Mater. Charact. 147 (2019) 464–511, http://dx.doi.org/10.1016/j.matchar.2018.06.019, URL https://www.sciencedirect.com/science/article/pii/S1044580318306636.

[25] J.E. Saal, S. Kirklin, M. Aykol, B. Meredig, C. Wolverton, Materials design and discovery with high-throughput density functional theory: The open quantum materials database (OQMD), JOM 65 (11) (2013) 1501–1509, http://dx.doi.org/10.1007/s11837-013-0755-4.

[26] S. Kirklin, J.E. Saal, B. Meredig, A. Thompson, J.W. Doak, M. Aykol, S. Rühl, C. Wolverton, The open quantum materials database (OQMD): assessing the accuracy of DFT formation energies, npj Comput. Mater. 1 (1) (2015) 15010, http://dx.doi.org/10.1038/npjcompumats.2015.10.

[27] A. Bieber, F. Ducastelle, F. Gautier, G. Tréglia, P. Turchi, Electronic structure and relative stabilities of $L1_2$ and $D0_{22}$ ordered structures occuring in transition metal alloys, Solid State Commun. 45 (7) (1983) 585–590, http://dx.doi.org/10.1016/0038-1098(83)90432-5, URL https://www.sciencedirect.com/science/article/pii/0038109883904325.

[28] C. Colinet, A. Pasturel, Ab initio calculation of the formation energies of $L1_2$, $D0_{22}$, $D0_{23}$ and one dimensional long period structures in $TiAl_3$ compound, Intermetallics 10 (8) (2002) 751–764, http://dx.doi.org/10.1016/S0966-9795(02)00054-7, URL https://www.sciencedirect.com/science/article/pii/S0966979502000547.

[29] C.M. Fang, Z. Fan, An ab initio study on stacking and stability of $TiAl_3$ phases, Comput. Mater. Sci. 153 (2018) 309–314, http://dx.doi.org/10.1016/j.commatsci.2018.07.011, URL https://www.sciencedirect.com/science/article/pii/S0927025618304397.